Pulsed EPR/ENDOR Characterization of Perturbations of the Cu_A Center Ground State by Axial Methionine Ligand Mutations

Claire E. Slutter,[†] Igor Gromov,[†] Boris Epel,[†] Israel Pecht,*[,‡] John H. Richards,[§] and Daniella Goldfarb*[,†]

Contribution from the Departments of Chemical Physics and Immunology, Weizmann Institute of Science, Rehovot, Israel 76100, and Division of Chemistry and Chemical Engineering, California Institute of Technology, Pasadena, California 91125

Received November 10, 2000. Revised Manuscript Received February 5, 2001

Abstract: The effect of axial ligand mutation on the Cu_A site in the recombinant water soluble fragment of subunit II of *Thermus thermophilus* cytochrome *c* oxidase ba_3 has been investigated. The weak methionine ligand was replaced by glutamate and glutamine which are stronger ligands. Two constructs, M160T0 and M160T9, that differ in the length of the peptide were prepared. M160T0 is the original soluble fragment construct of cytochrome ba_3 that encodes 135 amino acids of subunit II, omitting the transmembrane helix that anchors the domain in the membrane. In M160T9 nine C-terminal amino acids are missing, including one histidine. The latter has been used to reduce the amount of a secondary T2 copper which is most probably coordinated to a surface histidine in M160T0. The changes in the spin density in the Cu_A site, as manifested by the hyperfine couplings of the weakly and strongly coupled nitrogens, and of the cysteine β-protons, were followed using a combination of advanced EPR techniques. X-band (∼9 GHz) electron-spin−echo envelope modulation (ESEEM) and two-dimensional (2D) hyperfine sublevel correlation (HYSCORE) spectroscopy were employed to measure the weakly coupled ^{14}N nuclei, and X- and W-band (95 GHz) pulsed electron−nuclear double resonance (ENDOR) spectroscopy for probing the strongly coupled ^{14}N nuclei and the β-protons. The high field measurements were extremely useful as they allowed us to resolve the T2 and Cu_A signals in the $g_\perp$ region and gave ^1H ENDOR spectra free of overlapping ^{14}N signals. The effects of the M160Q and M160E mutations were: (i) increase in $A_\parallel(^{63,65}Cu)$, (ii) larger hyperfine coupling of the weakly coupled backbone nitrogen of C153, (iii) reduction in the isotropic hyperfine interaction, a_{iso}, of some of the β-protons making them more similar, (iv) the a_{iso} value of one of the remote nitrogens of the histidine residues is decreased, thus distinguishing the two histidines, and finally, (v) the symmetry of the **g**-tensor remained axial. These effects were associated with an increase in the Cu−Cu distance and subtle changes in the geometry of the Cu_2S_2 core which are consistent with the electronic structural model of Gamelin et al. (Gamelin, D. R.; Randall, D. W.; Hay, M. T.; Houser, R. P.; Mulder, T. C.; Canters, G. W.; de Vries, S.; Tolman, W. B.; Lu, Y.; Solomon, E. I. *J. Am. Chem. Soc.* **1998**, *120*, 5246−5263).

Introduction

Cytochrome *c* oxidase (COX) is a transmembrane protein complex which catalyzes the dioxygen reduction in the electron-transport chain of aerobic respiration. This enzyme's catalytic reaction cycle involves the sequential transfer of four electrons from cytochrome *c* to yield two H_2O molecules. Coupled to this cycle is a pumping action which translocates four protons/cycle to the intermembrane (periplasm) space of the mitochondria (bacterial cell), creating a proton gradient across the membrane. Discharge of this biological capacitor via a free diffusion of protons through the ATP synthase complex is then coupled to ATP synthesis.[1] The three-dimensional (3D) structure of COX from a number of different species has been determined.[3−5] All of these enzymes contain three transition metal sites; the initial electron acceptor, which accepts the electrons from cytochrome *c*, is a binuclear, copper valence delocalized center ($S = {}^1/_2$) called Cu_A, which cycles between an oxidized [Cu(1.5)Cu(1.5)] and a reduced [Cu(1)Cu(1)] state. The next sites in the intramolecular electron-transfer (ET) chain are the heme *a* center and the final catalytic site, bimetallic, Cu_B−heme a_3, where oxygen is bound and reduced. Each copper in Cu_A has a distorted tetrahedral geometry: Cu_1 is coordinated by a histidine imidazole, a cysteine thiolate, and a methionine thioether, whereas Cu_2 has a similar coordination sphere where the thioether is replaced with a main chain carbonyl of glutamine. The recently solved 3D structure of nitrous oxide reductase (N_2OR), which also contains a Cu_A site, shows the same structural characteristics with the exception that the main chain carbonyl is from a tryptophan.[6]

[†] Department of Chemical Physics, Weizmann, Institute of Science.
[‡] Department of Immunology, Weizmann, Institute of Science.
[§] California Institute of Technology.

(1) Musser, S. M.; Stowell, M. H. B.; Chan, S. I. In *Advances in Enzymology*; Meister, A., Ed.; John Wiley & Sons, Inc.: New York, 1995, pp 79−208.
(2) Iwata, S.; Ostermeier, C.; Ludwig, B.; Michel, H. *Nature* **1995**, *376*, 660−669.
(3) Tsukihara, T.; Aoyama, H.; Yamashita, E.; Tomizaki, T.; Yamaguchi, H.; Shinzawa-Itoh, K.; Nakashima, R.; Yaono, R.; Yoshikawa, S. *Science* **1995**, *269*, 1069−1074.
(4) Tsukihara, T.; Aoyama, H.; Yamashita, E.; Tomizaki, T.; Yamaguchi, H.; Shinzawa-Itoh, K.; Nakashima, R.; Yaono, R.; Yoshikawa, S. *Science* **1996**, *272*, 1136−1144.
(5) Wilmanns, M.; Lappalainen, P.; Kelley, M.; Sauer-Erksson, E.; Saraste, M. *Proc. Natl. Acad. Sci. U.S.A.* **1995**, *92*, 11955−11959.
(6) Brown, K.; Tegoni, M.; Prudêncio, M.; Pereira, A. S.; Besson, S.; Moura, J. J.; Moura, I.; Cambillau, C. *Nat. Struct. Biol.* **2000**, *7*, 191−195.

10.1021/ja003924v CCC: $20.00
Published on Web 05/10/2001

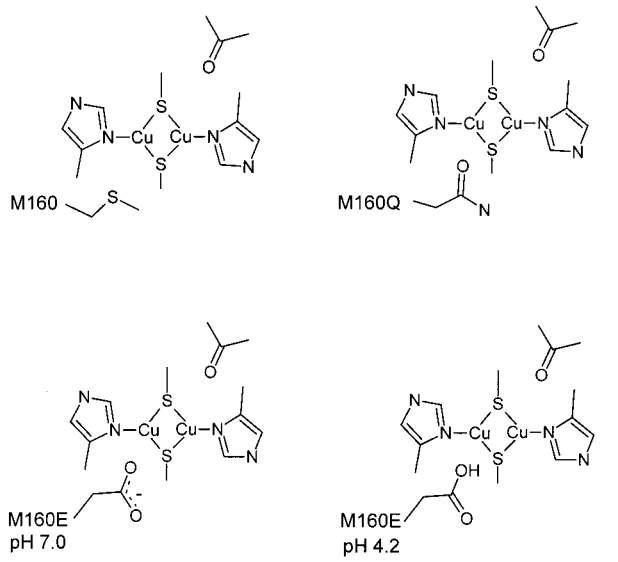

Figure 1. A schematic representation of the Cu_A site in *wt*, M160T0-(T9), and the M160QT0, M160ET0 (pH = 4.2, pH = 7.0) proteins.

The discovery of a binuclear copper center, whose function is ET, has been rather surprising, considering the abundant and well-characterized mononuclear type 1 (T1) copper site, which is prevalent in blue oxidases and azurins.[7] The evolutionary transition from a mononuclear to a binuclear ET site has been ascribed to the larger charge delocalization which results in a lower reorganization energy involved in electron transfer.[8−12] In addition, Gamelin et al.[9] have suggested that the ET properties of the Cu_A center may be better controlled by subtle changes in the core geometry and axial ligand interactions.

To simplify spectroscopic and electron-transfer investigations of the Cu_A center, a recombinant water soluble fragment of subunit II of *Thermus thermophilus* cytochrome *c* oxidase ba_3 that encodes 135 amino acids of subunit II and contains the Cu_A site has been expressed,[13] and its 3D structure has been determined.[14] Recently, we have reported stable mutations of the weak axial ligand, M160Q and M160E (see Figure 1), in this wild type (*wt*) Cu_A center.[16] These mutations resulted in a change in the intensities of the S-to-Cu charge-transfer bands at 480 to 530 nm in the optical spectra and a blue-shift of the higher-energy partner of this doublet, thus indicating a subtle change in the Cu_A center geometry while retaining the delocalized $S = {}^1/_2$ character. In those mutants, increasing strength of the weak ligand shifts more spin density from the ligands, mainly the S's, to the Cu atoms. In a manner analogous to that of the T1 centers, we expect that these observed alterations of the ground-state molecular orbital (MO) are relevant for understanding not only the changes in the absorption spectra but also the modulation of the reorganization energy, λ, and the redox potential. The axial ligand mutants may serve as a possible structural model for the modulation of the Cu_A center induced by cytochrome *c* binding. The role of fine-tuning of the electronic ground state may be illustrated by an interesting model for control of the ET reactivity of Cu_A via the axial ligand which has evolved from the analysis of 3D structure of bovine COX: Tsukihara et al.[4] have pointed out that Glu198 which provides its carbonyl as axial ligand is also sharing its carboxylate as ligand to the Mg^{2+} ion which is bound to the enzyme. Hence, these authors propose that "an oxidation state-linked conformational change, which controls the electron-transfer pathway between Cu_A and heme *a*, is operative".

To characterize in detail the effects induced by the axial ligand mutation on the Cu_A center we followed the changes in the spin density of the site as manifested by the hyperfine couplings of the weakly and strongly coupled nitrogens and of the cysteine β-protons. X-band (~9 GHz) electron-spin−echo envelope modulation (ESEEM) and two-dimensional (2D) hyperfine sublevel correlation (HYSCORE) spectroscopies were applied to the weakly coupled ^{14}N nuclei, and X- and W-band (95 GHz) pulsed electron−nuclear double resonance (ENDOR) spectroscopy to the strongly coupled ^{14}N nuclei and the β-protons. The results were then analyzed in terms of the model of Gamelin et al.[9] We found that the soluble fragment, M160T0, contained significant amounts of a secondary type 2 (T2) copper center, the signals of which interfered with the spectral analysis of the Cu_A center. To alleviate this problem and determine the source of this secondary site a second construct, M160T9, in which nine C-terminal amino acids are missing, including one histidine, was expressed and investigated as well.

Materials and Methods

Protein Preparation. Overexpression of the recombinant soluble fragment of subunit II of *Thermus thermophilus* containing the Cu_A center using a T7 RNA polymerase-based overexpression system has been described elsewhere.[13] Two constructs, M160T0 and M160T9, that differ in the length of the encoded peptide were prepared. The protein purification method used is a slight modification of the previously published protocol: After IPTG-induction of a 1 L cell culture, the cells were sedimented. The pellet was resuspended in 50 mL of buffer (50 mM Tris-HCl, pH 8) and lysed by sonication. The cell debris was removed by centrifugation, and $CuSO_4$ was added to the supernatant to a final concentration of 1 mM. Reconstitution of the Cu_A center for both the *wt* and mutant proteins occurs rapidly under these conditions. The reconstituted extract is equilibrated with 50 mL of buffer (100 mM phosphate/500 mM NaCl, pH 7.0) loaded directly onto a metal affinity column (HiTrap IMAC) loaded with Cu(II). The heat treatment and pH precipitation steps of the original protocol have been eliminated because the mutants have lower copper affinity and are less resilient to these harsher treatments. The protein is eluted with 10 mM imidazole in buffer (100 mM phosphate/500 mM NaCl, pH 7). As expected, the T0 constructs have higher affinity for the IMAC column than the T9, and a fraction of the protein precipitates on the column and cannot be recovered. The T9 construct does not exhibit this behavior. *Wt* is stable in 10 mM imidazole for several days, but the mutants are more sensitive and lose copper within several hours. Therefore, all proteins were kept in liquid nitrogen after preparation. After elution, a desalting HiTrap column equilibrated with 10 mM phosphate/200 mM NaCl, pH 7.0 was used to rapidly remove the imidazole. (Attempts to elute the protein by other methods (pH drop and NH_4Cl) were unsatisfactory as they resulted in a very broad elution profile and high final volumes.) The samples were concentrated by lyophilization or ultrafiltration. EPR samples were typically 1.5−3.0 mM Cu_A in 50% glycerol and 50% 100 mM phosphate/200 mM NaCl, pH 7.

(7) Reinhammar, B. Laccase. In *Copper Proteins and Copper Enzymes*; Lontie R., Ed.; CRC Press: Boca Raton, Fl, 1982; Vol 3, pp 1−35.
(8) Farver, O.; Lu, Y.; Ang, M. C.; Pecht, I. *Proc. Natl. Acad. Sci. U.S.A.* **1999**, *96*, 899−902.
(9) Gamelin, D. R.; Randall, D. W.; Hay, M. T.; Houser, R. P.; Mulder, T. C.; Canters, G. W.; de Vries, S.; Tolman, W. B.; Lu, Y.; Solomon, E. I. *J. Am. Chem. Soc.* **1998**, *120*, 5246−5263.
(10) Randall, D. W.; Gamelin, D. R.; LaCroix, L. B.; Solomon, E. I. *J. Biol. Inorg. Chem.* **2000**, *5*, 16−29.
(11) Blackburn, N., J.; de Vries, S.; Barr, M. E.; Houser, R. P.; Tolman W. B.; Sanders D.; Fee, J. A. *J. Am. Chem. Soc.* **1997**, *119*, 6135−6143.
(12) Larrson, S.; Källebring, B.; Wittung, P.; Malmström, B. G. *Proc. Natl. Acad. Sci. U.S.A.* **1995**, *92*, 7167−7171.
(13) Slutter, C. E.; Sanders, D.; Wittung, P.; Malmström, B. G.; Aasa, R.; Richards, J. H.; Gray, H. B.; Fee, J. A. *Biochemistry* **1996**, *35*, 3387−3395.
(14) Williams, P. A.; Blackburn, N. J.; Sanders, D.; Bellamy, H.; Stura, E. A.; Fee, J. A.; McRee, D. E. *Nat. Struct. Bio.* **1999**, *6*, 509−516.
(15) Nar, H.; Messershmidt, A.; Huber, R.; van de Kamp, M.; Canters, G. W. *J. Mol. Biol.* **1991**, *221*, 765−772.
(16) Slutter, C. E.; Gromov, I.; Richards, J. H.; Pecht, I.; Goldfarb, D. *J. Am. Chem. Soc.* **1999**, *121*, 5077−5078.

Mutagenesis. The M160QT0 and M160ET0(T9) mutations were introduced using a polymerase chain reaction (PCR) protocol. The final product of this PCR reaction is cleaved with Nde I and BamH I and cloned into the Pet9a plasmid as described previously.[13] The N-terminal portion of the coding sequence was amplified with a sense primer (5′ CTTTAAGAAGGAGATATA**CATAGT**GCCTACA 3′) and a mutagenic antisense primer (5′ TTAGCAGCC**GGATCC***TAC*CTCCTTCACCACGAT CGTGCCAA/GAC/GCTT 3′), yielding a 414 base pair (bp) insert after digestion. (Restriction sites are shown in bold, start and stop codons are underlined, and the mutated site is boxed.) A two-temperature PCR cycle was used. Each reaction had a 2 min preheat at 96 °C, 30 cycles of 30 s at 96 °C and 1 min at 72 °C, and a 5 min final extension at 72 °C. In a reaction volume of 100 μL, 0.2 mg of plasmid template, 25 pmol of each primer, 10 mM of each nucleotide, and BMB PCR buffer and Taq polymerase were used. Commercially available T7 promoter and T7 terminator primers were used to screen for the presence of the insert, yielding a 559 bp reaction product. Here a toothpick was used to resuspend some cells from an agar plate into 25 mL of doubly distilled H_2O. These cells were then transferred directly to the PCR tube. Amplification required 55 cycles, and the fragments were run on a standard agarose gel. Positive colonies were then sequenced. To verify that secondary mutations had not been introduced in the PCR reaction, both strands of the gene were sequenced completely.

EPR Measurements. Continuous wave (CW) X-band (9.13 GHz) EPR measurements were performed on a Varian E-12 spectrometer using standard variable temperature accessories. All *g*-values were calibrated relative to a DPPH standard. An Air Products Helitran flow system was used for the 11 K measurements

X-band ESEEM, HYSCORE, and ENDOR experiments were carried out at ~9.3 or ~8.5 GHz and 4−10 K, using a home-built spectrometer.[17] Field-sweep echo-detected (FS-ED) EPR spectra were recorded using the two-pulse echo sequence with $\pi/2$ and π pulses of 0.02 and 0.04 μs, respectively. The ESEEM measurements were done using the three-pulse sequence, $\pi/2-\tau-\pi/2-T-\pi/2-\tau-$echo, where the echo intensity is measured as a function of the time interval *T*. Typically, the $\pi/2$ pulse length was 0.02 μs and *T* was incremented in steps of 0.02 μs. HYSCORE spectra were recorded using the sequence $\pi/2-\tau-\pi/2-t_1-\pi-t_2-\pi/2-\tau-$echo, where the echo is measured as a function of t_1 and t_2.[18] The duration of the $\pi/2$ and π pulses was 20 ns, and the amplitude of the π pulse was twice that of the $\pi/2$ pulses. The increment in t_1 and t_2 was 0.04 μs and (130 × 130) points were collected. The appropriate phase cycles, eliminating unwanted echoes, were employed in all experiments.[19,20]

The ESEEM and HYSCORE data were treated with the Bruker WINEPR software. Prior to Fourier transformation (FT) of the ESEEM data, the background decay was removed by a polynomial fit. The resulting time domain traces were convoluted with a Hamming window, zero filling was performed, and after FT the magnitude mode was selected. The ESEEM spectra of the individual τ values were then summed to yield the final spectrum. In the HYSCORE data the background decay in both t_1 and t_2 dimensions was removed using a polynomial fit, the data were then convoluted with a Hamming or sinebell function, and after zero-filling to 512 points in each dimension, FT was carried out in the two dimensions. The spectra shown are contour plots in magnitude mode with a linear scaling of the contour intervals.

X-band ENDOR spectra were collected using the Davies ENDOR sequence:[21]

$$\begin{array}{ll} \text{MW} & \pi-T-\pi/2-\tau-\pi-\tau-\text{echo} \\ \text{RF} & \pi \end{array}$$

employing a probe head based on a bridged loop-gap resonator.[22] Typical RF pulse durations in the range of 4.5−5.5 μs were employed.

W-band FS-ED EPR spectra were recorded at 4.3 K using a home-built spectrometer[23] and the two-pulse echo sequence with pulse durations of 0.80 and 0.160 μs, respectively, and τ = 0.25 μs. The magnetic field in the W-band measurements was calibrated using the ^{1}H Larmor frequency determined from the ENDOR experiments. The probe-head used for the ^{1}H W-band measurements was similar to that described earlier,[23] whereas the ^{14}N measurements were obtained using a similar probe-head with the exception of a new RF coil (saddle coil with 10 turns instead of 4) optimized for measurements in 5−40 MHz frequency range and with a typical RF π-pulses of 25−30 μs for ^{14}N.[24]

Simulations. EPR simulations were carried out using the program developed by Neese,[25] and the HYSCORE spectra were simulated using program TRYSCORE.[26] In the following we present a brief description of the interactions considered and the definitions of the parameters used in TRYSCORE. The Hamiltonian for an unpaired electron, $S = {}^1/_2$, coupled to *n* nuclear spins is:

$$H = \beta\vec{B}\cdot\mathbf{g}\cdot\hat{S} + \sum_{i=1}^{n}(-\beta_n g_{ni}\vec{B}\cdot\hat{I}_i + \hat{I}_i\cdot\mathbf{A}_i\cdot\hat{S} + \hat{I}_i\cdot\mathbf{Q}_i\cdot\hat{I}_i) \quad (1)$$

The various terms in eq 1 represent electron Zeeman, nuclear Zeeman, superhyperfine, and quadrupole interactions, respectively, and the index *i* refers to a particular nucleus. The copper hyperfine interaction is neglected as it does not affect the ESEEM frequencies.[27] The principal components of $\mathbf{A}_i$, which for simplicity is assumed to be axially symmetric, are $A^p_{\perp i}$, $A^p_{\perp i}$, $A^p_{\parallel i}$. The isotropic part is given by $a_{\mathrm{iso}i}$ and the anisotropic component by $a_{\perp i}$ such that $A_{\perp i} = a_{\mathrm{iso}i} - a_{\perp i}$ and $A_{\parallel i} = a_{\mathrm{iso}i} + 2a_{\perp i}$. The principal values of the quadrupole tensor, $\mathbf{Q}_i$, are $Q^p_{zzi} = e^2qiQ/2I(2I-1)h$, $Q^p_{xxi} = -1/2Q^p_{zzi}(1-\eta_i)$ and $Q^p_{yy} = -1/2Q^p_{zzi}(1+\eta_i)$ where η is the asymmetry parameter, $\eta = (Q^p_{xx} - Q^p_{yy})/Q^p_{zz}$ for $|Q^p_{zz}| \geq |Q^p_{yy}| \geq |Q^p_{xx}|$. The orientation of the external magnetic field, $\vec{B}$, with respect to principal axis system of **g** is given by the polar and azimuthal angles θ_o and ϕ_o. The principal axis system of $\mathbf{A}_i$, is transformed into that of **g** by the polar and azimuthal angles θ_i and ϕ_i and that of $\mathbf{Q}_i$, by the Euler angles α_i, β_i, γ_i.

A single ^{14}N nucleus exhibits six ESEEM frequencies, three for each M_S manifold. Two correspond to $\Delta M_I = \pm 1$, $\nu^{\alpha,\beta}_{\mathrm{sq}1}$, $\nu^{\alpha,\beta}_{\mathrm{sq}2}$, and $\nu^{\alpha,\beta}_{\mathrm{dq}}$ to a double quantum transition, $\Delta M_I = \pm 2$. At X-band frequencies, weakly coupled ^{14}N nuclei often fulfill the cancellation condition where a_{iso} is approximately twice the nuclear Larmor frequency ($|a_{\mathrm{iso}}| \approx 2\nu_N$).[28,29] In this case the effective magnetic field experienced by the nucleus in one of the M_S manifolds is approximately zero. The ESEEM frequencies within this manifold are then close to the ^{14}N nuclear quadrupole resonance (NQR) frequencies, ν_0, ν_-, and ν_+ given by

$$\nu_\pm = \frac{3e^2qQ}{4h}\left(1 \pm \frac{\eta}{3}\right), \quad \nu_0 = \frac{e^2qQ}{2h}\eta \quad (2)$$

These frequencies appear as relatively narrow, orientation independent peaks in the ESEEM spectrum where $\nu_0 + \nu_- = \nu_+$ and $\nu^{\alpha,\beta}_{\mathrm{dq}}$ is approximated by:[30]

$$\nu^{\alpha,\beta}_{\mathrm{dq}} \cong 2\left[\left(\nu_N \pm \left|\frac{a_{\mathrm{iso}}}{2}\right|\right)^2 + \left(\frac{e^2qQ}{4h}\right)^2(3+\eta^2)\right]^{1/2} \quad (3)$$

Equation 3 is valid also when the cancellation condition is not fulfilled.

(17) Shane, J. J.; Gromov, I.; Vega, S.; Goldfarb, D. *Rev. Sci. Instrum.* **1998**, *69*, 3357−3364.
(18) Höfer, P.; Grupp, A.; Nebenführ, H.; Mehring, M. *Chem. Phys. Lett.* **1986**, *132*, 279−282.
(19) Fauth, J.-M.; Schweiger, A.; Braunschweiler, L.; Forrer, J.; Ernst, R. R. *J. Magn. Reson.* **1986**, *66*, 74−85.
(20) Gemperle, C.; Aebli, G.; Schweiger, A.; Ernst, R. R. *J. Magn. Reson.* **1990**, *88*, 241−256.
(21) Davies, E. R. *Phys. Lett. A.* **1974**, *47A*, 1−2.
(22) Forrer, J.; Pfenninger, S.; Eisengger, J.; Schweiger, A. *Rev. Sci. Instrum.* **1990**, *61*, 3360−3367.
(23) Gromov, I.; Krymov, V.; Manikandan, P.; Arieli, D.; Goldfarb, D. *J. Magn. Reson.* **1999**, *139*, 8−17.
(24) Epel, B.; Goldfarb, D. *J. Magn. Reson.* **2000**, *146*, 196−203.
(25) Nesse F. Electronic Structure and Spectroscopy of Novel Copper Chromophores in Biology. Ph.D Thesis, University of Konstanz, 1997.
(26) Szosenfogel, R.; Goldfarb, D. *Mol. Phys.* **1998**, *95*, 1295−1308.
(27) Mims, W. B. *Phys. Rev. B*, **1972**, *B5*, 2409−2419; **1973**, *B6*, 3543−3545.
(28) Mims, W. B.; Peisach, J. *J. Chem. Phys.* **1978**, *69*, 4921−4930.
(29) Flanagan, H. L.; Singel, D. J. *J. Chem. Phys.* **1987**, *87*, 5606−5616.
(30) Dikanov, S. A.; Tsvetkov, Yu.D.; Bowman, M. K.; Astashkin, A. V. *Chem. Phys. Lett.* **1982**, *90*, 149−153.

Table 1. Distances of the β-Protons from the Two Cu and S Atoms in the Cu_A Core and the Orientations of the Corresponding X_i-H_j Vectors with Respect to the $g_{||}$ Direction

proton	Sc_{153} θ_{ij}, ϕ_{ij}, r(Å)	Sc_{149} θ_{ij}, ϕ_{ij}, r(Å)	Cu_1 θ_{ij}, ϕ_{ij}, r(Å)	Cu_2 θ_{ij}, ϕ_{ij}, r(Å)
$H1_{C153}$	17.2, 254.0, 2.37	55.2, 93.4, 3.96	37.9, 136.9, 3.03	35.9, 48.4, 2.96
$H2_{C153}$	35.3, 140.8, 2.37	68.4, 102.5, 5.27	60.1, 128.4, 4.14	54.0, 84.3, 3.53
$H1_{C149}$	118.7, −83.4, 4.89	165.7, −34.6, 2.42	132.6, 253.7, 3.27	126.9, −51.2, 3.67
$H2_{C149}$	111.1, 255.7, 5.20	142.5, 213.1, 2.36	115.6, 229.3, 4.03	122.4, −87.0, 3.24

In the HYSCORE simulation program the frequencies and transition probabilities are obtained from the numerical diagonalization of the Hamiltonian matrix. The above approximate equations were used for qualitative analysis of the spectra and for obtaining starting values for the simulations.

^{1}H ENDOR spectra were simulated using a program developed in our laboratory according to Erickson et al.[31] based on the Hamiltonian presented in eq 1. In this program **A** is not limited to axial symmetry and its anisotropic part, given by **D**, was calculated from the atomic coordinates as described by Neese.[25] For each cysteine β-proton denoted by i, $\mathbf{D}_i$ is obtained from contributions of four $\mathbf{D}^p_{i,j}$ ($j = 1,4$) matrixes, corresponding to the individual H_i-X_j interactions where $X_j = Cu_1$,-Cu_2,S_1,S_2. The principal values of each $\mathbf{D}^p_{i,j}$ are $(-a_{\perp ij}, -a_{\perp ij}, 2a_{\perp ij})$ where $-a_{\perp ij} = (\mu_0/4\pi)\rho_j g_n \beta_n g \beta/(hr^3_{H_i-X_j})$ and ρ_j is the spin density on X_j. The individual $\mathbf{D}_i$'s, expressed in the principal axis system of **g**, are then obtained by summing over all four dipolar interactions according to:

$$\mathbf{D}_i = \sum_{j=1}^{4} \mathbf{D}_{ij} = \sum_{j=1}^{4} R(\theta_{ij},\phi_{ij}) \mathbf{D}^p_{ij} R^{-1}(\theta_{ij},\phi_{ij}) \qquad (4)$$

where θ_{ij},ϕ_{ij} are the polar and azimuthal angles representing the orientation of the X_i-H_j vector with respect to the **g** coordinate system, $R(\theta_{ij},\phi_{ij})$ is the corresponding rotation matrix, and $\mathbf{D}^p_{ij}$ is given in its principal axis system. As in the HYSCORE simulations, θ_0 and ϕ_0 describe the orientation of $\vec{B}$ with respect to the **g** principal axis system.

The orientation of g_{zz} was taken along the bisector of the two vectors normal to the $S_{C153}-Cu_1-S_{C149}$ and $S_{C153}-Cu_2-S_{C149}$ planes and that of g_{yy} along the $S_{C153}-S_{C149}$ direction.[25,32] The various θ_{ij},ϕ_{ij} and r_{X_j-Hi} were calculated from the atomic coordinates of the 3D structure,[14] and the protons were placed using InsightII by MSI. Table 1 lists the distances and angles obtained.

Results

CW EPR Measurements. The CW EPR spectrum of the *wt Thermus* Cu_A fragment, recorded at 11 K, is presented in Figure 2A. It shows, in addition to the typical spectrum of the Cu_A center, weak low field signals characteristic of a T2 copper center.[7] At 150 K this signal becomes more evident, and a fine structure of ^{14}N superhyperfine splittings appears on the $M_I(^{63,65}Cu) = -3/_2$ feature (around 325 mT). At this temperature the contributions from Cu_A are reduced considerably due to its faster spin−lattice relaxation, T_1. The EPR parameters of this T2 Cu(II) are $g_\perp = 2.04$, $g_{||} = 2.3$, $A_{||}$ (^{63,63}Cu) = 17.3 mT, and $A(^{14}N) \approx 1.5$ mT. These parameters and the five line pattern of the ^{14}N hyperfine splitting are consistent with a Cu(II) coordinated to two imidazole groups. The T2 signal intensity is considerably reduced in M160T9, where nine C-terminal amino acids, including a histidine, are missing (Figure 2A). In M160T9 the Cu_A signal can be observed also at 150 K (Figure 2B), and in the 11 K spectrum the $A_{||}(^{63,63}Cu)$ features of Cu_A are better resolved (Figure 2A). This suggests that the presence of the T2 center affects the spin lattice relaxation time, T_1, of the Cu_A center. Furthermore, the surface histidine (H39), deleted in M160T9, may be a ligand of the T2 center in M160T0, and its elimination disrupts this center.

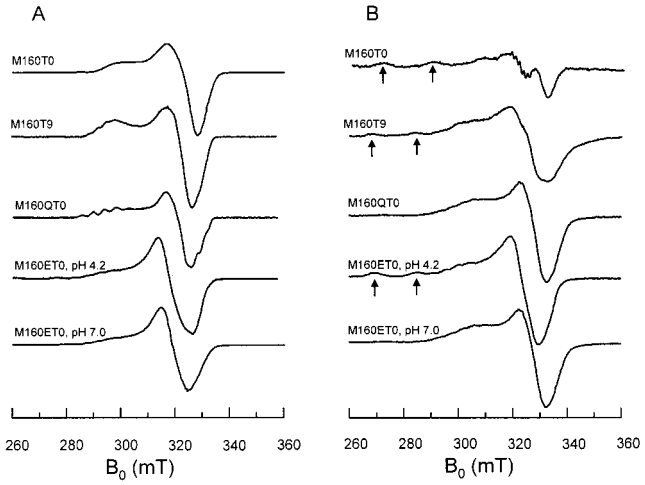

Figure 2. X-band EPR spectra of the different Cu_A proteins investigated (as labeled on the Figure) recorded at (A) 11 K and (B) 150 K. The arrows mark the $A_{||}$ features of the T2 signal.

Table 2. Hyperfine and g-Values of the Investigated Cu_A Centers

construct	$A_{||}$, mT[16]	g_x, g_y[a]	g_z[a]
M160T0(T9)	3.1	2.000, 2.014 (1.99, 2.0)[b]	2.189 (2.17)
M160QT0	4.2	2.021 (2.02, 2.02)	2.176 (2.19)
M160ET0(T9)	4.2	2.026 (2.00, 2.05)	2.175 (2.20)
T2 (M160ET9)	17.3	2.063	2.302

[a] Values determined from the simulations of the W-band spectra. [b] The values in brackets correspond to g_x, g_y, and g_z as determined from earlier X-band simulations.[16]

The EPR spectra of the two axial ligand mutants, M160QT0, pH 7.0, and M160ET0, pH 4.2 and pH 7.0, are also shown in Figure 2. The most salient features of these spectra compared to the M160T0(T9) spectra is the presence of a larger, better resolved ^{63,65}Cu hyperfine interaction and a more intense Cu_A signal at 150 K. While the M160QT0 sample is almost free of the T2 signal, its presence in the M160ET0 samples is significant. Although at pH 4.2 this mutant is expected to have a protonated side chain, while at pH 7 it should be deprotonated (see Figure 1), the only difference between the two M160ET0 spectra is the lower resolution of the hyperfine structure at pH 7. The EPR parameters of the samples investigated are summarized in Table 2.[16] In contrast to M160T0, the Cu_A signal in both M160ET0 samples can be observed also at 150 K in the presence of T2. This suggests that at least part of the T2 and the Cu_A centers are in different protein molecules due to some loss of Cu from the Cu_A site because of lower affinity induced by the mutation. This is supported by the relatively large amount of the secondary T2 found in M160ET9.

A better separation of the overlapping powder patterns of the T2 and Cu_A spectra is obtained at W-band where the $g_\perp$ singularities of T2 and Cu_A are well resolved. The X- and W-band FS-ED EPR spectra of M160T9 are compared in Figure 3A,B. The relative amount of the Cu_A and T2 centers, 62:38,

(31) Erickson, R. *Chem. Phys.* **1996**, *202*, 263−275.
(32) Neese, F.; Zumft, W. G.; Antholine, W. G.; Kroneck, P. M. H. *J. Am. Chem. Soc.* **1996**, *118*, 8692−8699.

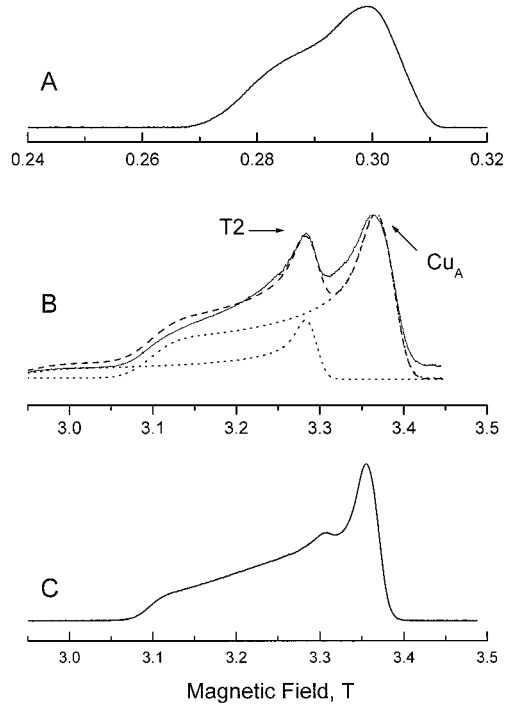

Figure 3. (A) X-band FS-ED EPR spectrum of M160T9 recorded at 10 K with $\tau = 0.250$ μs. (B) W-band FS-ED EPR spectra of M160T9. The dotted traces represent the individual contributions of Cu_A and T2, and the dashed trace is their sum (62:38 ratio, respectively). (C) The W-band FS-ED EPR spectrum of M160QT0. The W-band spectra were recorded at 5 K with $\tau = 0.4$ μs.

was determined by simulations of the W-band spectrum. The simulated spectrum, represented by a dashed trace in Figure 3B, is a superposition of two spectra calculated using the parameters listed in Table 2, and the dotted traces show their individual contributions. The W-band spectrum shows that the amount of T2 present is not as negligible as it may seem from the X-band spectra.[35] The M160QT0 sample (Figure 3C), which shows no detectable T2 signal in the X-band spectrum, exhibits only a weak T2 signal in the W-band spectrum. The M160ET0 W-band spectrum (not shown in Figure 3) is similar to that of M160T0. The W-band spectra provide clear evidence that all the Cu_A centers examined have an axial or nearly axial **g**-tensor. This confirms our earlier suggestion that the rhombic appearance of the M160ET0 X-band EPR spectrum is due to the presence of the overlapping T2 signal.[16]

Three-Pulse ESEEM. The weakly coupled ^{14}N nuclei in the Cu_A center were probed by ESEEM spectroscopy. Orientation-selective measurements did not show significant frequency shifts in any of the samples over the accessible field range. Accordingly, we present only the spectra recorded at a field corresponding to maximal echo intensity, near $g_\perp$. Figure 4A shows three-pulse ESEEM spectra of M160T0 and M160T9 where each spectrum is a summation of several individual traces recorded with different τ values to overcome blind-spots.[27] The ESEEM spectrum of M160T0 includes signals at ~0.8 1.6 and ~4.2 MHz, marked with dotted arrows in Figure 4A, which are characteristic for the imidazole remote nitrogen that fulfills the cancellation condition. The first two frequencies correspond

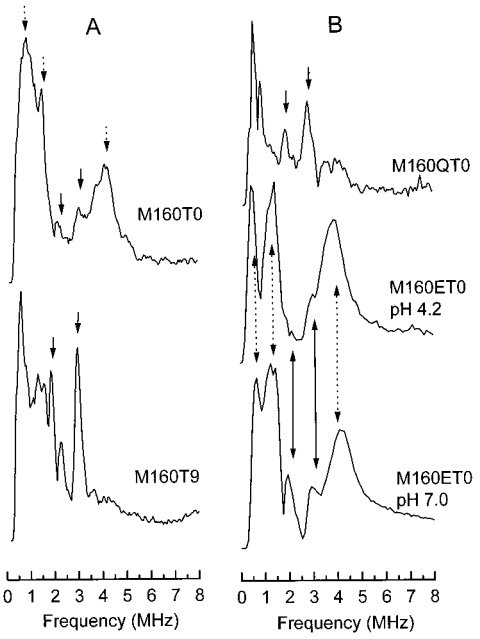

Figure 4. Sum ESEEM spectra of (A) M160T0 and M160T9 ($\tau = 0.15-0.30$ μs, step 0.05 μs, $B_0 = 296.6$ mT), (B) M160QT0 ($\tau = 0.15-0.3$ μs, step 0.05 μs, $B_0 = 293$ mT) and M160ET0, pH = 4.2, 7.0 ($\tau = 0.18-0.3$ μs, step 0.04 μs + trace of $\tau = 0.4$ μs). All spectra were recorded at a spectrometer frequency of 8.4 GHz and $T = 4.2$ K. The solid arrows mark the signals due to Cu_A, whereas the dotted arrows mark those of the T2 center.

to the NQR frequencies, $\nu_o \approx \nu_-$ and ν_+, and the third to ν_{dq}.[36-38] In addition, two weak lines appear at 2.1 and 2.9 MHz (see solid arrows on the figure). These two peaks are more intense in the M160T9 spectrum while the other lines are significantly weaker. We therefore assign the 2.1 and 2.9 MHz peaks to the Cu_A site and the others to the T2 center. The Cu_A site also has signals in the 0−1 MHz region that overlap with those of the T2. These results, along with the CW EPR data show that the T2 Cu(II) is coordinated by a surface histidine(s) and exogenous imidazoles. The ESEEM spectrum of the M160QT0 mutant at pH 7.0 (Figure 4B) shows that it is free of the T2 ^{14}N nuclei, in agreement with the X- and W-band EPR spectra. The ^{14}N frequencies of the Cu_A center appear at 1.8, 2.10, and 2.8 MHz. In contrast to M160QT0, the spectra of M160ET0 at pH 4.2 and pH 7.0 (Figure 4B) are dominated by the T2 ^{14}N signals. Nonetheless, despite their presence, Cu_A signals are visible at 2.0 and 2.9 MHz at both pHs.

HYSCORE Measurements and Simulations. The congestion of the 1D ESEEM spectra caused by overlapping ^{14}N signals arising from different ^{14}N nuclei complicates their assignments, and therefore HYSCORE measurements were carried out as well. Figure 5A shows the HYSCORE spectrum of M160T0 recorded at maximal echo intensity. It shows two pairs of cross-peaks at (0.7,3.8), (1.4,4.2) MHz, labeled T2 in the figure, which are assigned to the $(\nu_{0,-},\nu_{dq})$ and (ν_+,ν_{dq}) peaks of the remote imidazole nitrogen of the T2 center. From these frequencies and eq 2 we obtained $\eta \approx 0.8-1$ and $e^2qQ/h = 1.4$ MHz, consistent with an imidazole bound to Cu(II).[36-39] Another set

(33) Gemperle, C.; Schweiger A. *Chem. Rev.* **1991**, *91*, 1481−1505.
(34) Coremans, J. W.; A.; Poluektov, O. G.; Groenen, E. J. J.; Warmerdam, G. C. M.; Canters G. W.; Nar, H.; Messerschmidt, A. *J. Phys. Chem.* **1996**, *100*, 19706−19713.
(35) Fee, J. A.; Sanders, D.; Slutter, C. E.; Doan, P. E.; Aasa, R.; Karpfors, M. Vänngård, T. *Biochem. Biophys. Res. Commun.* **1995**, *212*, 77−83.
(36) Goldfarb, D.; Fauth, J.-M.; Farver, O.; Pecht, I. *Appl. Magn. Reson.* **1992**, *3*, 333−351.
(37) Goldfarb, D. *Electron Spin Resonance, A Specialist Periodical Report*; Atherton, N. M., Davies, M. J., Gilbert, B. C., Eds.; The Royal Society of Chemistry: UK 1996; Vol. 15, p 182 and references therein.
(38) Jiang, F.; McCracken, J.; Peisach, J. *J. Am. Chem. Soc.* **1990**, *112*, 9035−9044.
(39) Jiang, F.; Karlin, K. D.; Peisach, J. *Inorg. Chem.* **1993**, *32*, 2576−2582.

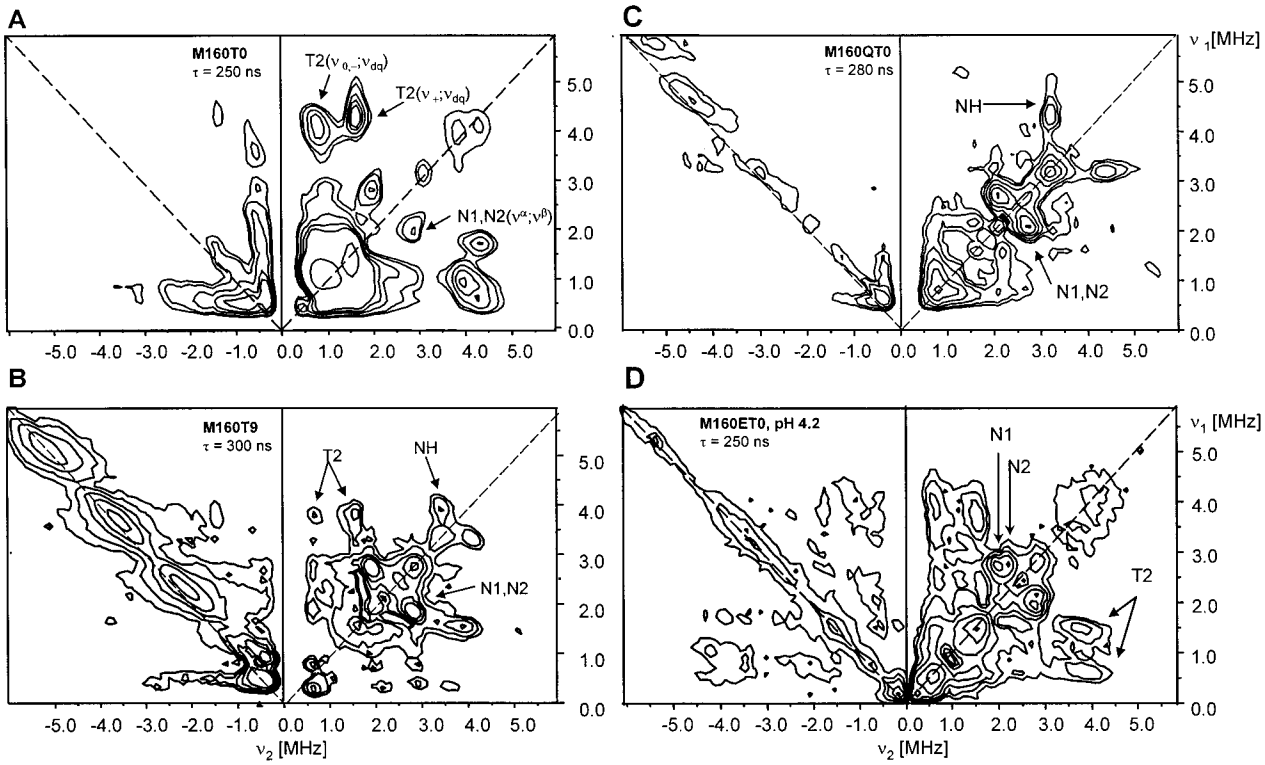

Figure 5. HYSCORE spectra (10 K) of: (A) M160T0 (B_0 = 327.6 mT, ν = 9.4 GHz, and τ = 0.25 μs), (B) M160T9 (B_0 = 295.0 mT, ν = 8.5 GHz, and τ = 0.30 μs), (C) M160QT0 (B_0 = 290.6 mT, ν = 8.7 GHz, and τ = 0.28 μs) and (D) M160ET0 pH = 4.2 (B_0 = 304.5 mT, ν = 8.68 GHz, and τ = 0.25 μs).

Table 3: Summary of the Frequencies of the HYSCORE Cross-Peaks (in MHz) in the Samples Studied

Cu_A center	N1($\nu^{\alpha}_{dq};\nu^{\beta}_{dq}$)	N2($\nu^{\alpha}_{dq};\nu^{\beta}_{dq}$)	NH($\nu^{\alpha}_{dq};\nu^{\beta}_{dq}$)	T2($\nu_{-,0},\nu_{dq}$)	T2($\nu_{+,0},\nu_{dq}$)
M160T9	1.9; 2.8	1.9; 2.8	3.3; 4.1	0.7; 4.2	1.5; 4.2
M160QT0	2.0; 2.7	2.2; 2.6	3.1; 4.3	−	1.6; 3.9
M160ET0, pH 4.2	2.0; 2.8	2.2; 2.8	−	0.6; 4.2	1.4; 4.2
M160ET0, pH 7.0	2.0; 2.7	2.2; 2.7	−	0.6; 4.2	1.4; 4.2

of cross-peaks at (1.9, 2.8) MHz is attributed to (ν^{α}_{dq}, ν^{β}_{dq}) of the remote ^{14}N of the imidazole group in Cu_A, referred to as N1/N2. Using eq 3, e^2qQ/h = 1.4 MHz and η = 0.7−0.9, a_{iso} is estimated to be 0.55−0.8 MHz, which is about one-half that of the T2 remote nitrogens. The ESEEM frequencies of N1/N2 are consistent with previous ESEEM studies of the Cu_A site of N_2OR where simulations gave a_{iso} = 0.6 MHz.[40] For comparison a_{iso} values of 1.3 and 0.87 MHz were reported for the two remote nitrogens in mononuclear T1 centers.[36,41] The HYSCORE spectrum of M160T9 recorded at maximal echo intensity, presented in Figure 5B shows all of the peaks discussed above, except that the T2 signals are significantly weaker, and additional cross-peaks, corresponding to (ν^{α}_{dq}, ν^{β}_{dq}) of another Cu_A nitrogen, are apparent at (3.3; 4.1) MHz (the intense signal on the diagonal of the (−,+) quadrant is due to noise). From these frequencies a e^2qQ/h value of 3−4 MHz is estimated. This value is characteristic of a backbone nitrogen, NH, as reported by Jin et al.[40] for N_2OR. A similar spectrum was observed for a higher field position, except that the T2 cross-peaks are weaker since its contribution at this field is lower.

The HYSCORE spectra of M160QT0 (Figure 5C) are free of the T2 cross-peaks, substantiating their assignment to a secondary site in the other preparations. The cross-peaks of N1/N2 exhibit some resolution and appear at (2.0, 2.7) and (2.2, 2.8) MHz. This indicates that, in contrast to *wt* Cu_A, the two remote nitrogens are slightly inequivalent. The NH cross-peaks appear at (3.1, 4.3) MHz, which is somewhat different from that of *wt* Cu_A, indicating a larger a_{iso} and a comparable quadrupole coupling constant. A similar resolution of the peaks of N1/N2 is observed in the spectra of M160ET0, pH = 4.2 (Figure 5D). These are accompanied by intense T2 cross-peaks that appear in the (+,+) and (−,+) quadrants. The NH signals, were not clear in any of the spectra measured, and it seems that the relatively large amount of T2 disturbs its detection. The spectrum of M160ET0, pH = 7.0 is similar to that of pH = 4.2, and it is not shown. HYSCORE cross-peaks observed in all investigated samples and their assignments to the various nitrogens are given in Table 3.

The hyperfine and quadrupole parameters of the weakly coupled ^{14}N nuclei were obtained from simulations of the HYSCORE spectra, and they are listed in Table 4. Figure 6A,B shows simulations of the HYSCORE spectra of N1/N2 in M160T9 and M160QT0. Those of M160ET0 pH 4.2 and 7.0 are similar to that of M160QT0, and therefore they are (not presented). The well-resolved features in the M160QT0 and M160ET0 cross-peaks could not be reproduced with a single set of hyperfine or quadrupole parameters. Simulated HYSCORE spectra of the NH of M160T9 and M160QT0 are shown in Figure 6C,D. The highest contour level in these spectra

(40) Jin, H.; Thomann, H.; Coyle, C. L.; Zumft, W. G. *J. Chem. Soc.* **1989**, *111*, 4262−4269.
(41) Coremans, J. W. A.; Poluektov, O. G.; Groenen, E. J. J.; Canters, G. W.; Nar, H.; Messerschmidt, A. *J. Am. Chem. Soc.* **1996**, *118*, 12141−12153.

Table 4. Best Fit Hamiltonian Parameters of the Weakly Coupled Nitrogens Obtained from the Simulations of the HYSCORE Spectra[a]

sample	Q(N1,N2), (±0.05) MHz	η(N1, N2), (±0.10)	a_{iso}(N1, N2) (±0.04) NHz	$a_\perp$(N1, N2) (±0.02) MHz
M160T9	1.40, 1.40	0.90, 0.90	0.51, 0.51	0.10, 0.10
M160Q	1.52, 1.30	0.94, 0.94	0.30, 0.48	0.10, 0.10
M160E, pH 4.2	1.52, 1.30	0.90, 0.90	0.36, 0.46	0.10, 0.10
M160E, pH 7.0	1.48, 1.28	0.90, 0.90	0.32, 0.42	0.10, 0.10

sample	Q(NH), MHz	η(NH)	a_{iso}(NH), MHz	$a_\perp$(NH), MHz
M160T9	3.09 ± 0.03	0.88 ± 0.01	0.80 ± 0.06	0.15 ± 0.01
M160QT0	3.08 ± 0.03	0.76 ± 0.01	1.14 ± 0.06	0.15 ± 0.01

[a] The spectra were not very sensitive to the values of polar angles of the hyperfine tensor. The values used in the simulations were $\theta = 0°$ and $\phi = 0°$. The Euler angles $\alpha = 0°$, $\beta = 45°$, $\gamma = 0°$ were used for the quadrupole tensor. The simulations were not sensitive to α and γ and to a ± 20° change in β. The integration range over θ_0 was 30−90° and over ϕ_0 0−180°.

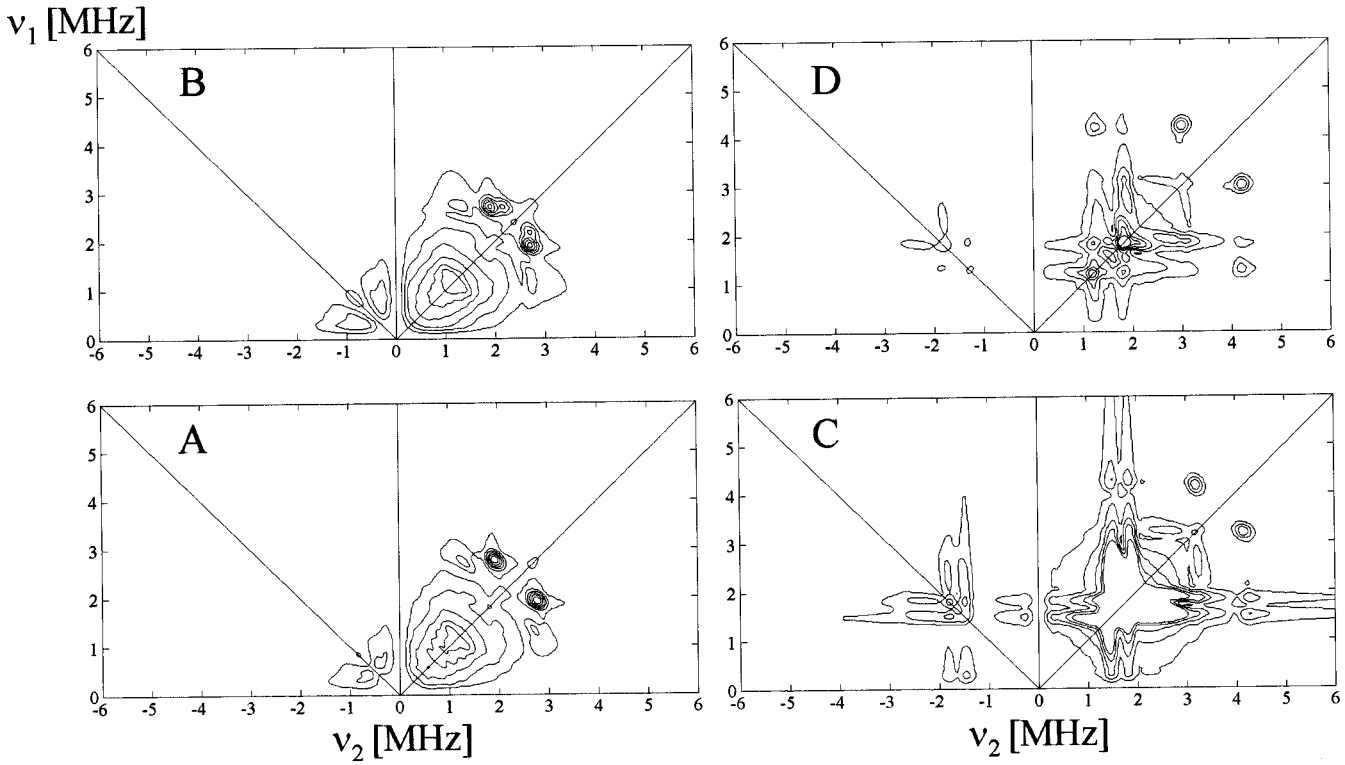

Figure 6. Simulated HYSCORE spectra of (A) N1/N2 of M160T9, (B) N1/N2 of M160QT0, (C) NH of M160T9, and (D) NH of M160QT0. The spectra were calculated with the hyperfine and nuclear quadrupole parameters listed in Table 3. The integration range over θ_0 was 30−90° and over ϕ_0 0−180°.

is a factor of 2−3 lower than that used in the N1/N2 spectra which is in agreement with the presence of two coupled imidazole nitrogens and one amide. These relative intensities are also observed experimentally in both the HYSCORE and ESEEM spectra. The values of e^2qQ/h and η we obtained from the simulations for N1/N2 and NH confirm their assignment to the remote[36−38] and amide nitrogen,[40,42] respectively.

ENDOR Measurements. M160T0, M160T9. The X-band ENDOR spectrum of M160T0, measured at the maximal echo intensity, consists of a doublet with a splitting of ∼12 MHz centered about the proton's Larmor frequency, ν_H (Figure 7a). The doublet is not symmetric, and its low-frequency component exhibits some structure with peaks at 7 and 9 MHz. Measurements at other magnetic fields within the EPR powder pattern show that the doublet center varies as would ν_H, whereas the peaks at 7 and 9 MHz remain practically unchanged. This suggests that the spectrum is a superposition of a ^{1}H doublet with a hyperfine splitting, $A(^1H)$, of ∼12 MHz and ^{14}N signals, appearing around $A(^{14}N)/2$. The two ^{14}N signals may correspond the two M_S manifolds split by $2\nu_N$ (∼2 MHz at X-band), yielding $A(^{14}N)$ ∼16 MHz. Alternatively, it could indicate two nitrogens with different A values. Furthermore, both the quadrupole and anisotropic hyperfine interactions can also contribute to the appearance of spectral features.

To substantiate the assignment of the ^{1}H and ^{14}N signals and obtain more accurate ^{1}H hyperfine couplings, W-band ENDOR measurements were carried out. At these frequencies the ^{1}H and ^{14}N signals are well separated. Moreover, the $g_\perp$ singularities of Cu_A and T2 are well-resolved at W-band so that interferences from the directly bound ^{14}N of T2 are eliminated. At X-band the signal of this ^{14}N is around 20 MHz,[44,45] overlapping with the high frequency component of the ^{1}H doublet. The ^{1}H region of the W-band ENDOR spectrum of M160T9 is shown in Figure

(42) Rabbani, S. R.; Edmonds, D. T.; Gosling, P. *J. Magn. Reson.* **1987**, *72*, 230−237.

(43) Coremans, J. W. A.; van Gastel, M.; Poluektov, O. G.; Groenen, E. J. J.; den Blaauwen, T.; van Pouderoyen, G.; Canters, G. W.; Nar, H.; Hammann, C.; Messerschmidt, A. *Chem. Phys. Lett.* **1995**, *235*, 202−210.

(44) Gurbiel, R. J.; Fann, Y. C.; Surerus, K. K.; Werst, M. M.; Musser, S. M.; Doan, P. E.; Chan; S. I.; Fee, J. A.; Hoffman, B. M. *J. Am. Chem. Soc.* **1993**, *115*, 10888−10894.

(45) Gromov, I.; Marcesini, A.; Farver, O.; Pecht, I.; Goldfarb, D. *Eur. J. Biochem.* **1999**, *26*, 820−830.

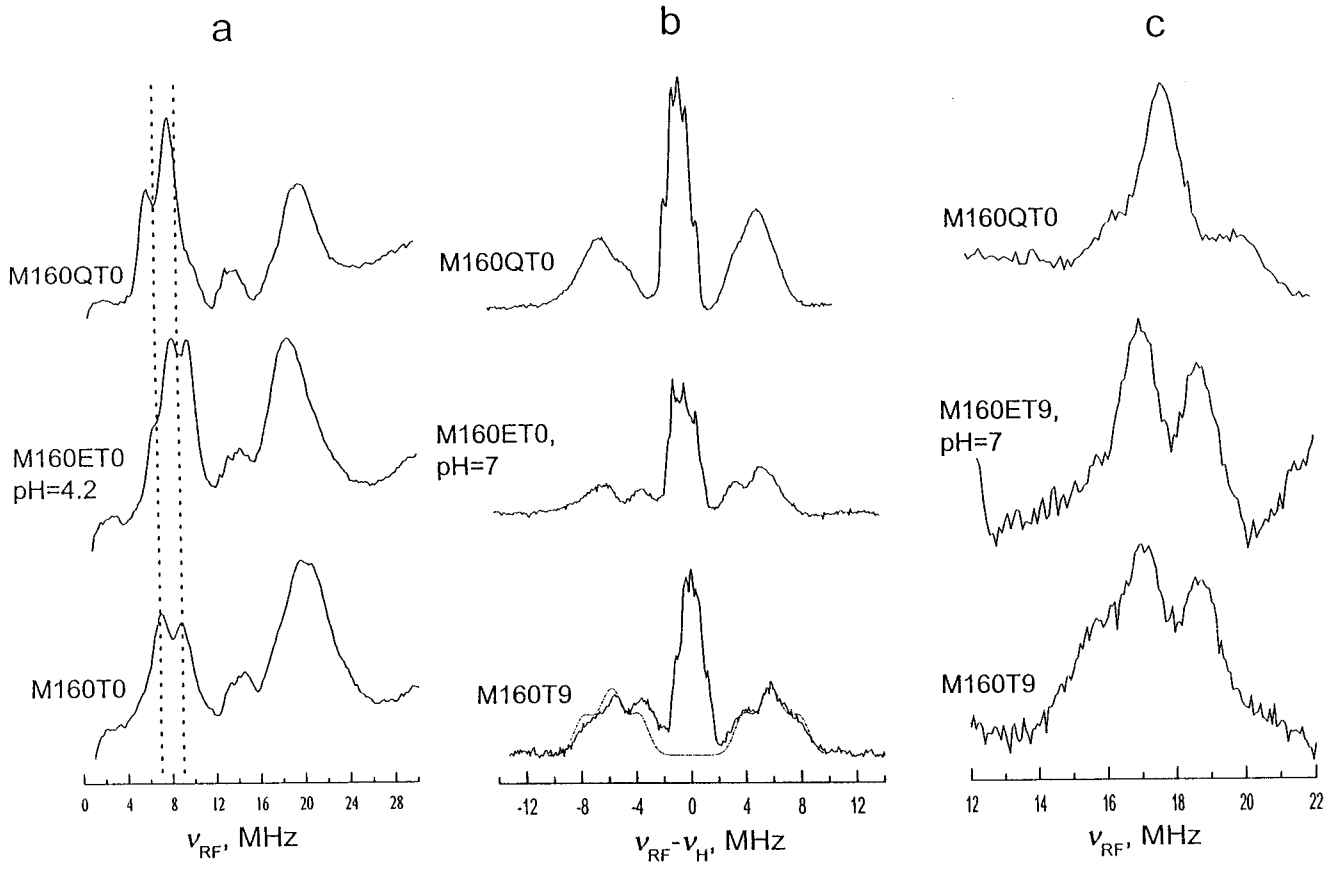

Figure 7. (a) X-band Davies ENDOR spectra of (a) M160T0, M160ET0 pH = 7, and M160QT0 (ν = 9.40 GHz, τ = 0.41, 0.46, 0.46 μs, respectively, MW pulses 0.04, 0.02, 0.04 μs). The positions of ^{14}N peaks of Cu M160T0 are marked by dotted lines; (b) ^{1}H W-band Davies ENDOR spectra of M160T9, M160ET9 pH = 7 and M160QT0 (τ = 0.4 μs, the frequency scale is relative to the ^{1}H Larmor frequency); (c) same as (b) for the ^{14}N region. All spectra were recorded at maximal echo intensity.

7b. As expected, the spectrum is symmetric with respect to ν_H and two groups of doublets can be identified. The first consists of those with small splittings (<3 MHz) that are due to weakly coupled protons and will not be discussed any further. These signals do not appear in the X-band spectrum since it was recorded with shorter MW pulses that are less selective. The second group of lines consists of well-resolved doublets with splittings of 8, 11.6, and 15.6 MHz and are assigned to the cysteine β-protons.

Using the procedure described in the simulation section we calculated from the 3D structure of the Cu_A soluble fragment[14] the anisotropic hyperfine matrix of each β-proton in the g-frame assuming a spin density of 20% for the sulfurs and 28% for the coppers.[47] Proton H1C153 was found to have the largest anisotropy (A_{zz} = 2.56 MHz), whereas for all other three, A_{zz} was in the range of 1.74−1.81 MHz. When the ENDOR spectrum is recorded at the $g_\perp$ position, the orientation of the principal axis system of the hyperfine interaction with respect to that of **g** determines their individual contributions to the inhomogeneous broadening. Simulations of the anisotropic hyperfine contributions of each of the protons at this field position, (taking a selected orientation range of θ_0 = 75−90°) showed that for H1C153 and H1C149 the width at half-height is ∼0.8 MHz and that of H2C153 and H2C149 is ∼1 MHz. This indicates that the spectral features observed are due to protons with different isotropic hyperfine interactions rather than powder pattern singularities of equivalent protons. Accordingly the ENDOR spectrum was simulated using the fixed anisotropic contributions discussed above and four different a_{iso} values as fitted parameters. The dotted trace shown in Figure 7b represents the best fit obtained with a_{iso}(H1C153) = −6.8, a_{iso}(H1C149) = −10.3, a_{iso}(H2C153) = −12.1, and a_{iso}(H2C149) = −15.3 MHz. The negative sign was necessary to reproduce the reduction in the splitting observed for spectra recorded close to $g_{||}$. The assignment of the various a_{iso} values to the specific protons was done taking into account their dependence on the HCSS dihedral angles[47] (see Discussion).

The ^{14}N region of the spectrum, shown in Figure 7c, exhibits two signals at 17.1 and 18.7 MHz and a shoulder at 15.7 MHz which are assigned to the high-frequency components of ^{14}N doublets centered about ν_N (10.3 MHz). The fine structure could arise from the anisotropy of the hyperfine or the quadrupole interactions, from the inequivalence of the two nitrogens, or from any combination of the three. Unfortunately, due to S/N limitations we were unable to record a series of orientation selective spectra that would have allowed a quantitative analysis of the ^{14}N hyperfine couplings. Nonetheless, the combination of X-band and W-band spectra can narrow down some of the above possibilities. Assuming that the two nitrogens are equivalent, the center of the spectrum can be used to estimate $a_{iso} \approx$ 13.8 MHz. This should yield X-band signals centered at 6.9 ± MHz, which are different from the 8 ± MHz signals observed. The alternative is to assume that the features at 17.1 and 18.7 MHz are due to two inequivalent nitrogens with a_{iso} values of 13.8 and 16.8 MHz. This should lead to X-band signals at approximately 6.8 ± 1 and 8.4 ± 1 MHz. Considering that

(46) Coremans, J. W. A.; Poluektov, O. G.; Groenen, E. J. J.; Canters, G. W.; Nar, H.; Messerschmidt, A. *J. Am. Chem. Soc.* **1997**, *119*, 4726−4731.

(47) Neese, F.; Kappl, R.; Hütterman, J.; Zumft, W. G.; Kroneck, P. M. H. *J. Bioinorg. Chem.* **1998**, *3*, 53−67.

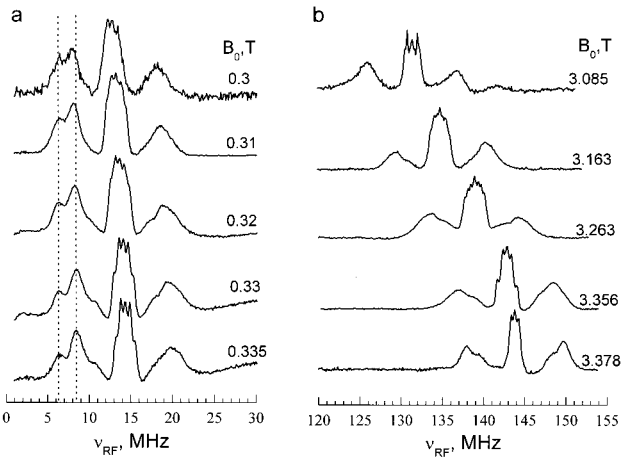

Figure 8. Orientation selected Davies ENDOR spectra of M160QT0 measured at (a) X-band (MW pulses 0.20, 0.10, 0.20 μs, $\nu = 9.43$ GHz, $\tau = 0.46$ μs). (b) W-band, the ^{1}H region (MW pulses 0.18, 0.09, 0.18 μs, $\nu = 9.43$ GHz, $\tau = 0.40$ μs).

the ^{14}N quadrupole interaction of the bound nitrogen is around 1−3 MHz[44,46] and the limited available data, we conclude that the hyperfine couplings of the two nitrogens is in the range of 13−17 MHz.

M160QT0, M160ET0(T9). The ^{1}H W-band ENDOR spectra of M160ET9, pH = 7, M160QT0, presented Figure 7b, show that mutation of the weak axial ligand affects the coupling of some of the β-protons. In M160ET9 the ±15.8 MHz shoulders disappear, and only two doublets with splittings of 8 and 11.6 MHz are resolved. The spectrum of M160QT0 also exhibits only two doublets, with 9 and 11.6 MHz splitting. The corresponding X-band spectra, shown in Figure 7a, are not too informative due to overlap with the ^{14}N signals. The ^{14}N spectrum of M160ET9 is rather similar to that of M160T9, whereas that of M160QT0 shows some differences (Figure 7c). The position of the lines suggest that the hyperfine couplings remain within the 13−17 MHz range which is in agreement with the position of the ^{14}N features in the X-band spectra, as shown in Figure 7a.

Since the amount of the T2 copper in M160QT0 was minimal, we were able to record good quality orientation selective ^{1}H X- and W-band ENDOR spectra, as shown in Figure 8. Both sets were recorded with long selective MW pulses, and therefore the signals of the weakly coupled protons are present. The features assigned to ^{14}N appear in all X-band spectra and exhibit a very mild field dependence as expected. The W-band spectra show that the hyperfine coupling of the β-protons are highly isotropic and that the maximum splitting of 11.6 MHz observed at $g_\perp$ decreases to 10.9 MHz at $g_\parallel$. This indicates that the anisotropic hyperfine is small as in the *wt*. This is further supported by the similarity of the line shape of the high-frequency doublet component in the X-and W-band spectra. The selected range of orientation at W-band is significantly smaller than at X-band due to the larger spread of the powder pattern, and therefore significant differences would have appeared in the case of large anisotropic hyperfine interactions. Considering that no marked conformational changes are expected to occur by the mutations, simulations carried out with the anisotropic hyperfine interactions calculated for *wt* Cu_A showed that a_{iso} has to be negative in order to reproduce a reduction in the splitting when the measuring point changes from $g_\perp$ to $g_\parallel$. This was taken into account in the simulations of *wt* Cu_A described earlier. Precise simulations of the W-band ENDOR spectra of the mutants were not attempted due to the large number of unknown parameters related to the anisotropic component of the hyperfine interaction of each β-proton.

Discussion

The Secondary T2 Site. The studied protein samples can be divided into a group that contains considerable amounts of T2 copper (M160T0, M160ET0, M160ET9) and that where T2 is a minor species (M160QT0, M160T9). The presence of a foreign Cu(II) center in the soluble fragment preparations of M160T0 has been noted previously,[35] although without characterization. The Cu(II) hyperfine interaction ($A_\parallel(^{63,65}Cu) = 17.3$ mT), the resolved ^{14}N superhyperfine structure in the M160QT0 150 K EPR spectrum and the intense NQR frequencies in the ESEEM spectra, show that the Cu(II) is coordinated to two imidazole groups. The presence of the T2 copper is disturbing since at X-band its EPR spectrum overlaps with the Cu_A signals and it interferes with the detection of the weakly coupled nitrogens in the Cu_A site. Thus, it was important to understand the nature of this T2 center to minimize its interference.

There are two sources of imidazole present in the sample: solvent-accessible surface histidines, H117 and H39, and the imidazole used to elute the protein from the metal affinity column. The presence of surface histidines may promote dimer formation, which has indeed been observed on nondenaturing gel analysis of the M160T0 preparations.[13] Thus, it is likely that the dimer formation nucleated by the T2 center is also responsible for bringing two Cu_A centers to proximity, thus increasing the electron relaxation rate in M160T0. The proximity of the T2 to Cu_A can also lead to enhanced relaxation. The removal of H39 in M160T9 diminishes, but does not completely eliminate, the T2 signal. Interestingly, in M160T9 the ^{63,65}Cu hyperfine splitting of Cu_A is well-resolved, and its signal can be observed also at 150 K. The residual T2 signal, present in the 150 K M160T9 spectrum, has an $A_\parallel(^{63,65}Cu)$ value that is still consistent with a Cu(II)/imidazole center. It could arise also from Cu(II) released from the Cu_A active site. This free Cu(II) could then bind to H117 and any other residual imidazole present from the metal affinity purification. The large amount of T2 Cu in M160ET0 and M160ET9, together with the presence of a strong Cu_A signal at 150 K, suggests that the mutation has led to a significant reduction in the copper binding affinity.

The other possible candidate for a T2 center with an imidazole ligand is the presence of a half-occupied Cu_A center or a valence-trapped Cu_A center. In this case, a Cu(II) species ligated to histidine and cysteine residues is expected. Such a center should exhibit a relatively low $A_\parallel(^{63,65}Cu)$ value due to the large covalency of the Cu−S bond. This is inconsistent with the observed high 17.3 mT value, typical of T2 coordinated to histidines and water. The possibility that in the half-occupied Cu_A center the Cu(II) is not coordinated to cysteine is highly unlikely, although it cannot be ruled out.

Assignment of Weakly Coupled Nitrogens. Two types of different weakly coupled nitrogens were detected in *wt* Cu_A: N1/N2 and NH. On the basis of the quadrupole coupling, N1/N2 were assigned to the remote nitrogen of the histidine residues and NH to a backbone nitrogen. In the mutants N1 and N2 could be distinguished as having slightly different hyperfine couplings (see Tables 3, 4), whereas in *wt* only one signal was detected. Hence, either N1 and N2 are magnetically equivalent, or only one of them exhibits a sufficiently large couplings to produce signals observed in the ESEEM/HYSCORE spectrum. The latter case is, however, inconsistent with the relative intensities of the N1/N2 and NH signals and the rather small range of

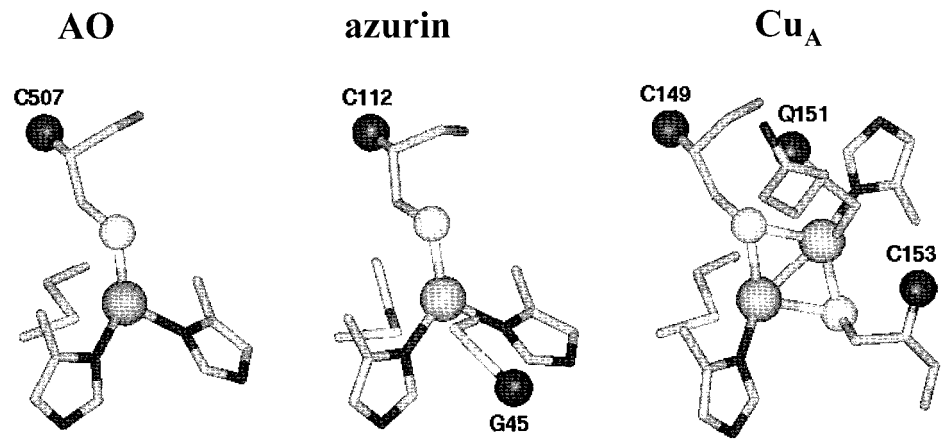

Figure 9. The 3D structure of the Cu_A site in *Thermus thermophilus* cytochrome *c* oxidase ba_3 drawn using the atomic coordinates given in[14] compared to that of the T1 center of Azurin[15] and AO.[55]

hyperfine coupling found for the directly coordinated nitrogens. This implies that the axial ligand mutation causes a reduction in a_{iso} of the ^{14}N that belongs to the histidine that is coordinated to the same copper as the mutated axial ligand, namely H114.[14] The relatively small values of a_{iso} are consistent with the reduced $^{63,65}Cu$ and bound ^{14}N hyperfine couplings as compared to those of T1.[44] The coupling parameters we obtained for N1, N2, and NH are similar to those reported by Jin et al. for the Cu_A site in N_2OR.[40] The latter study, however, also reports the presence of an another remote imidazole nitrogen with coupling parameters similar to those observed for T2. Our results are not consistent with the presence of such a nitrogen in the Cu_A site. Considering the significantly smaller spin density on the coppers compared to that in T1 and T2 sites, it is hard to rationalize such a large coupling. Hence, we suspect that also in N_2OR it originates from a T2 center.

The assignment of the backbone NH to a specific residue in the structure is not straightforward as in N1/N2. Nonetheless, the assignment to a specific amide is essential for understanding the effect of axial ligand mutation on the spin density distribution in the center because its a_{iso} is highly sensitive to the mutations; it increased from 0.9 MHz in M160T0 to 1.08 MHz in M160QT0. Examining the 3D structure of *wt* M160T0[14] we have noted the distances of amide nitrogens from the Cu_2S_2 core and the number of bonds separating them from the coppers and sulfurs which have large spin densities.[9,47] The closest backbone nitrogens are: Q151NH of one of the axial ligands, and C153NH (Figure 9). C153NH is within 3.5 Å of two atoms in the core (N−Cu_2, 3.41 Å; N−C153S, 3.10 Å) and three bonds away from C153S, whereas Q151NH is 3.67 Å from C149S and three bonds away from Cu_2. Interestingly, the cysteine side chains show a marked dissimilarity, placing C153NH close to the core while orienting C149NH away, directed toward the hydrophobic core. The possibility that the NH cross-peaks in the M160QT0 HYSCORE spectrum are due to the δ-amide of the Q axial ligand is excluded because a change in the ^{14}N quadrupole coupling constant compared to *wt* would be expected due to the different nitrogen environments in $-CO-NH_2$ and $-CO-NH-$. Therefore, on the basis of its closest proximity to the Cu_2S_2 core we assign the weakly coupled NH to C153NH.

A weakly coupled backbone ^{14}N with $a_{iso} = 0.95$ MHz, $e^2qQ/h = -3.1$, and $\eta = 0.4$ was also reported for the T1 copper of azurin.[41,43] This ^{14}N exhibits HYSCORE cross-peaks at (2.8,3.9) MHz, similar to those of NH in the *wt* Cu_A.[48] The azurin amide was assigned to the backbone nitrogen of the cysteine ligand,[41,43] although an alternative assignment to the Gly45 amide has also been suggested.[48] Due to the delocalization of the unpaired electron over the two coppers in Cu_A, it would be expected that the coupling of a cysteine backbone nitrogen will be about half that of the azurin, unless they have a significantly different distance or orientation with respect to the Cu. The orientations of the cysteine residues in the T1 centers of azurin and ascorbate oxidase (AO) and in the Cu_A fragment are compared in Figure 9. The orientation of C149NH relative to C149S and Cu_1 is very similar to that in azurin, thus ruling out the possibility that it is the weakly coupled NH. In contrast, the orientation of C153NH is significantly different, substantiating the amide assignment to C153NH.

This assignment is also supported by the recently published 3D structure of N_2OR[6] where a weakly coupled amide with quadrupole and hyperfine parameters similar to those found in the present work was observed.[40] In N_2OR the backbone nitrogen of C565 has a similar orientation with respect to the Cu_2S_2 core, positioning it close to Cu_1 (3.43 Å) and to the sulfur of C565, similar to C153 in *wt* Cu_A. Moreover, the backbone nitrogen of the other cysteine, C561, is also directed away from the core. Interestingly, a similar orientation of the two cysteine residues with respect to the core was also found in the Cu_A site of Bovine heart COX[4] and the engineered site of quinol oxidase.[5]

Analysis of the β-Proton Couplings. Neese et al. have shown that the a_{iso} values of the β-protons in the Cu_A site depend on the HCSS dihedral angle,[25,47] θ, according to

$$a_{iso} = B\rho_s[C/B + \cos^2(\theta + \phi)] \qquad (5)$$

where $\phi = 0, 90°$ for a $^2B_{2u}$ or a $^2B_{3u}$ ground state, respectively, and ρ_s corresponds to the spin density on the sulfur. The *C* and *B* values represent the efficiency at which the spin density is transferred to the $C^\beta H_2$ moiety and they depend on structural factors such as the orientation of $S^\gamma-C^\beta$ with respect to the Cu−S−S−Cu plane (ψ) and the $S^\gamma-S^\gamma-C^\beta$ angle (δ).[49] These, in principle can be different for the two cysteines.[49] For simplicity we have fitted the experimental a_{iso} values to one set of *B* and C values as we cannot unambiguously assign the observed couplings to specific protons. Earlier reports showed that the ground state is $^2B_{3u}$[32,37,49] and therefore the a_{iso} values of the four β-protons of M160T0(T9), obtained from the simulations of the W-band ENDOR spectra, were fitted to eq 5 with $\phi =$

(48) Kofman, V.; Farver, O.; Pecht, I.; Goldfarb, D. *J. Am. Chem. Soc.* **1996**, *118*, 1201−1206.

(49) Salgado, J.; Warmerdam, G.; Bubacco, L.; Canters, G. W. *Biochemistry* **1998**, *37*, 7378−7389.

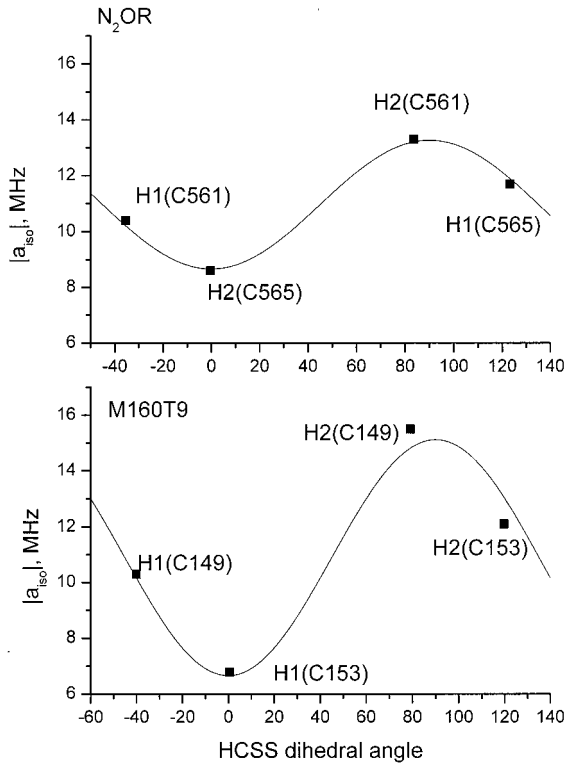

Figure 10. The dependence of the absolute value of a_{iso} of the β-protons of (a) M160T0(T9)[14] and (b) N_2OR[6] on the HCSS dihedral angle for $\phi = 90°$.

90° as shown in Figure 10a. The dihedral angles were obtained from the 3D structure of the soluble Cu_A fragment.[14] Assuming $\rho_s = 0.2$[47] we obtain $B = -46.2$ and $C = -33.2$ MHz.

The a_{iso} values of the β-protons of N_2OR (8.6, 10.4, 11.7, and 13.3 MHz) are quite close in magnitude to those of M160T9.[47] Using the recently reported 3D structure of N_2OR[6] we correlated them with the dihedral angles as shown in Figure 10b. Interestingly, the dihedral angles seem to be conserved. Thus, the difference between the proteins originate in the *B* and C values, namely in the ψ and δ angles. Four different hyperfine couplings, 10.5, 7.5, 9.4, 2.1 MHz, were also found for the Cu_A site in the soluble domain of subunit II of COX of *Paraccocus versutus* using room-temperature paramagnetic NMR measurements.[49] One of these values is significantly smaller than any of our values. The reason for this discrepancy maybe be the different measurement temperature, 4−5 K in our case, and room temperature for the NMR measurements, where contributions from excited states may be significant.

The overall effect of the axial ligand mutations on a_{iso} of the β-protons is that they become more equivalent. A change in the spin density on the sulfurs would result in scaling up or down of all protons, which is not observed. The M160ET9 mutation caused a selective decrease in the magnitude of a_{iso} of mainly one proton (−15.3 to ∼−13 MHz), whereas in M160QT0 one increased (−6.8 to −7.3 MHz) and another decreased (−15.3 to ∼−13 MHz). A change of −20° in the dihedral angle of the β-protons of C149 could account for the changes observed in the ENDOR spectrum. Alternatively, they may be due to a change in the values of *B, C* induced by subtle alteration in the core geometry along with a change in ρ_s. Considering the very close (conserved) dihedral angles of the β-protons in the Cu_A site in the *wt* soluble fragment, N_2OR, bovine heart COX[4], and the engineered site of quinol oxidase,[5] a change of −20° seems unlikely, and therefore we presume that a combination of a small change in the dihedral angle and in the core geometry takes place. The ENDOR frequencies of the β-protons of M160QT0 are close to those of N_2OR,[47] while the dihedral angles of the latter are very similar to those of the M160T0, thus supporting minor changes in the core conformation in the latter. For example, the hinge angle in M160T0 is 171° ,[14] while in N_2OR it is 149.2°.[6] We note, however, that only a limited change in the hinge angle is possible since according to the Neese et al.[32] an angle larger than 150° should result in a nonaxial *g*-tensor which we have not observed.

Effect of Axial Ligand Mutation on the Spin-Density. The changes in the Cu_A site attributed to the mutation of the weak methionine axial ligand with a stronger ligand, glutamine, or glutamic acid are summarized as follows: (i) the $^{63,65}Cu$ hyperfine of both coppers increased, (ii) the isotropic hyperfine coupling of the amide of C153 increased in the M160Q mutant, (iii) a_{iso} of some of the cysteine β-protons decrease, and the overall spread of the a_{iso} values decreased, making them more equivalent, (iv) the a_{iso} value of one of the remote nitrogens of the histidine ligands decreased, and the two histidine ligands can be distinguished, and (v) the symmetry of the *g*-tensor remained axial. These provide the first set of experimental data that allows a detailed examination of the effect of the weak axial ligand on the ground-state properties of Cu_A site. These results can therefore be interpreted in terms of the model of Gamelin et al.[9,10] and enable the evaluation of its validity.

Using a combination of electronic spectroscopies supported by MO calculations on several Cu_A centers and two synthetic model copper thiolate dimers, one mixed valence and the other homovalent, Gamelin et al.[9] described the electronic structure of the Cu_A center. In this description they pointed out the relevance of valence delocalization and axial ligand interaction for modulation of the electronic structure and control of both the redox potential and the ET reorganization energy. In this model the metal interaction with the axial ligand plays an important role. The Cu_A has a σ^* type HOMO (highest occupied molecular orbital) involving a significant Cu−Cu interaction. The σ^* character is, in turn, responsible for stabilization of the delocalized ground state of Cu_A, while the charge delocalization has been the key issue in lowering the reorganization energy. This has been recently demonstrated experimentally by the analysis of the internal ET in native COX[50] and by the enhanced rate of the intramolecular ET in an engineered purple Cu_A azurin, as compared to that in the native T1 site in azurin, despite a smaller ET driving force for the Cu_A.[8] The increase in the σ^* character at the expense of the π character can be achieved by a decreased Cu−Cu distance (compression of the Cu_2S_2 core) and weakening of the axial ligand interaction. In addition, the position of the equatorial nitrogen ligand of the histidine residues with respect to the Cu_2S_2 core is also important. The effect of the axial ligand can be summarized as follows: a weakened axial interaction results in an increase in the Cu−Cu bonding and an increased charge donation from the equatorial His ligands.[9,10]

Our results show that the axial ligand has a small but significant effect on the spin distribution in the Cu_A center, which reflects on the ground-state wave function. In general our results agree with the model of Gamelin et al.[9,10] In the mutants, where the strength of one axial ligand has increased relative to the native site, a decrease in the Cu−Cu bonding was observed. This in turn should lead to a decrease in the S spin density and an increase in the Cu spin density as indeed

(50) Farver, O.; Einarsdóttir, Ó.; Pecht, I. *Eur. J. Biochem*. **2000**, *267*, 1−6.

observed by the $A_{||}(^{63,65}Cu)$ increase. The spin density, α^2, in the Cu $-|A_1;x^2 - y^2\rangle - |A_2;x^2 - y^2\rangle$ molecular orbital can be estimated using the approach outlined by Neese.[25] The values obtained were α^2(M160T9) = 0.30−0.32 and α^2(M160QT0) = α^2(M160ET0) = 0.35−0.37, where each of the coppers contributes 50%. The mutation leads to an increase of ∼5% in the total Cu spin density. The above were calculated using the EPR values listed in Table 2 and average values of $A_\perp(^{63,65}Cu)$ = 42 MHz and $A_\perp(^{63,65}Cu)$ = 42.5 MHz for M160T9 and M160QT0, respectively, as determined from X-band EPR simulations and neglecting the **A** rhombicity. The range of α^2 is a consequence of using the somewhat different *g*-values obtained from the X-band or W-band simulations.

The strengthening of an axial ligand should also be associated with a reduction in the spin density on the imidazole ligand. Our results allowed only rough estimates of the hyperfine couplings of the coordinated nitrogens which do not resolve the effect of the mutation. Nonetheless, a decrease in the spin density in one of the His ligands could be inferred from the reduction in a_{iso} of one of the remote nitrogens in M160QT0 and M160ET0. The ratio between a_{iso} of the bound and remote nitrogens of the imidazole nitrogens in copper complexes is fairly constant. For example, in the T1 ligands the ratios are 19.3, 21 for azurin[41,46] and 20, 21 for stellacyanin.[51] Accordingly, a reduction in the spin density of one of the bound nitrogens should be proportional to reduction in the remote nitrogen of the same residue. Because we could not determine the anisotropic hyperfine interaction of the bound ^{14}N, the total spin density on the this nitrogen cannot be estimated.

The reduction in the S spin-density should lead to a general decrease in the hyperfine couplings of all the β-protons. In addition, the decrease in the Cu−Cu bonding is associated with a rotation of the Cu σ^* HOMO from a σ^* to a π character which also involves a rotation of the sulfur *p* orbitals. In turn, this rotation should affect the couplings of the β-protons because their orientation with respect to the sulfur *p* orbitals may become less or more favorable. This effect may be similar to that expected from a change in the HCSS dihedral angle caused by small conformational change. Our results do not show a uniform change in the hyperfine couplings of all protons that can be ascribed exclusively to the reduction in the S spin density, but rather suggest a combination of all three effects mentioned above. If we assume that the reduction in the S spin density is the major reason for the reduction of a_{iso} of the β-proton with the largest $|a_{iso}|$ from 15.3 to ∼13 MHz, a change of about 3% in the spin density is obtained (taking the spin density of each sulfur in *wt* as 20%[47]).

The relatively large increase of the hyperfine coupling of C153NH in M160QT0 is rather surprising, considering the predicted decrease in the S spin density and the reduction in hyperfine couplings of some protons. Hence, we associate the increase in a_{iso} with a conformational change that makes hyperconjugation more effective and a decrease the distance to the C153S or Cu_2. In terms of spin densities, the increase in a_{iso} amounts to a change in the 2s spin density from 0.05 to 0.07%.

Finally it is interesting to compare the effects of axial ligand mutations on the mononuclear analogue, the T1 Cu(II) site. The results published so far have concentrated primarily on the 3D structure and the effect on the rhombicity of **g**. Unfortunately, there are no data regarding the hyperfine couplings of ligand nuclei. Romero et al.[52] have described the M121Q mutant as a distorted tetrahedral geometry where the oxygen of the Q121 axial ligand forms a stronger bond to Cu (2.26 Å), and the distance between the copper and the main chain carbonyl oxygen of Gly45 lengthens to 3.37 Å, making this interaction too weak to consider this atom as a ligand. Relative to *wt* azurin, the Cu also moves 0.26 Å out of the plane of equatorial ligands (C112, H114 and H46) toward the oxygen of of Q121. Karlsson et al.[53] have described the ligand field alterations in M121E azurin for both the protonated and deprotonated side chains. The O−Cu distance in M121E azurin at pH 4.0, 2.21 Å, is comparable to the axial M121Q distance. Similarly, the geometry is a distorted tetrahedron with the Cu pulled out of the equatorial plane and the Gly45 interaction weakened (3.4 Å). All of these were associated with an increase in the rhombicity of the *g*-matrix due to significant spin-density transfer to the stronger axial ligand.[34] A recent investigation of the M121H mutant of azurin shows, however, that the **g**-tensor remains axial although the new ligand is a strong one.[54] Finally, an important difference between the Cu_A and T1 centers should be noted. In the former the Cu−S core structure and the terminal histidine ligands limits the conformational changes at the Cu atom near the mutated axial ligand, which most probably inhibits deviation from axiality.

Acknowledgment. This work has been supported by the German−Israel Foundation for Scientific Research (D.G. and I.P.), National Institutes of Health Grant GM16424 (J.H.R.), and a Feinberg Postdoctoral Fellowship (C.E.S.). C.E.S is deeply indebted to Dr. Angelo Di Bilio, Professor Mike Hill and Professor Harry Gray for numerous discussions about electron transfer, COX, and Cu_A. We thank Dr. Kieron Brown for making the N_2OR coordinates available for us and Professor Peter M. H. Kroneck for the many preprints and the help in getting the N_2OR coordinates. We are grateful to Dr. Frank Neese for the EPR simulation program.

JA003924V

(51) Thomann, H.; Bernardo, M. *Methods Enzymol.* **1993**, *227*, 118−189.

(52) Romero, A.; Hoitink, C. W. G.; Nar, H.; Huber, R.; Messerschmidt, A.; Canters, G. W. *J. Mol. Biol.* **1993**, *229*, 1007−1021.

(53) Karlsson, B. G.; Tsai, L.-C.; Nar, H. Sanders-Loehr, J.; Bonander, N.; Langer, V.; Sjölin, L. *Biochemistry* **1997**, *36*, 4089−4095.

(54) van Gastel, M.; Canters, G. W.; Krupka, H.; Messerschmidt, A.; de Waal, E. C.; Warmerdam, G. C. M.; Groenen, E. J. J. *J. Am. Chem. Soc*. **2000**, *122*, 2322−2328.

(55) Messerschmidt, A.; Ladenstein, R.; Huber, R.; Bolognesi, M.; Avigliano, L.; Petruzzelli, R.; Rossi, A.; Finazzi-Agro, A. *J. Mol. Biol.* **1992**, *224*, 179−205.